

Data Smashing 2.0: Sequence Likelihood (SL) Divergence For Fast Time Series Comparison

Yi Huang, Ishanu Chattopadhyay

Institute of Genomics and Systems Biology and

Department of Medicine, University of Chicago, Chicago, IL, 60637, USA

{yhuang10, ishanu}@uchicago.edu

Abstract—Recognizing subtle historical patterns is central to modeling and forecasting problems in time series analysis. Here we introduce and develop a new approach to quantify deviations in the underlying hidden generators of observed data streams, resulting in a new efficiently computable universal metric for time series. The proposed metric is *universal* in the sense that we can compare and contrast data streams regardless of where and how they are generated, and without any feature engineering step. The approach proposed in this paper is conceptually distinct from our previous work on data smashing [4], and vastly improves discrimination performance and computing speed. The core idea here is the generalization of the notion of KL divergence often used to compare probability distributions to a notion of divergence in time series. We call this the sequence likelihood (SL) divergence, which may be used to measure deviations within a well-defined class of discrete-valued stochastic processes. We devise efficient estimators of SL divergence from finite sample paths, and subsequently formulate a universal metric useful for computing distance between time series produced by hidden stochastic generators. We illustrate the superior performance of the new smash2.0 metric with synthetic data against the original data smashing algorithm, and other state of the art tools, *e.g.* dynamic time warping [23]. Pattern disambiguation in two distinct applications involving electroencephalogram data and gait recognition is also illustrated. We are hopeful that the smash2.0 metric introduced here will become an important component of the standard toolbox used in classification, clustering and inference problems in time series analysis.

Index Terms—Universal Metric; Data Smashing; Beyond Dynamic Time Warping; Probabilistic Finite Automata; Time Series Clustering

1 INTRODUCTION

Efficiently learning stochastic processes is a key challenge in analyzing time-dependency in domains where randomness cannot be ignored. For such learning to occur, we need to define a distance metric to compare and contrast time series. Examples of such metrics from the literature include the classical l_p distances and l_p distances with dimensionality reduction [18], the short time series distance (STS)[20], which takes into account of irregularity in sampling rates, the edit based distances[21] and generalizations to continuous sequences[6], and the dynamic time warping (DTW)[23], which is used extensively in the speech recognition community. However these distance metrics mentioned all have either or both of the following limitations: first, dimensionality reduction and feature selection heavily relies on domain knowledge and inevitably incur trade-off between precision and computability. Most importantly, it necessitates the attention of human experts and data scientists. Secondly, when dealing with data from non-trivial stochastic process dynamics, state of the art techniques might fail to correctly estimate the similarity or lack thereof between exemplars. For example, suppose two sequences

recording n tosses of a fair coin, use 1 to represent a head and 0, tail. The two sequences are extremely unlikely to share any similarity on the face value, *i.e.* they have a large pointwise distance, but they are generated by the same process. A good measure of similarity should strive to disambiguate the underlying processes. The Smash2.0 metric introduced here addresses both these limitations.

When presented with finite sample paths, the Smash2.0 algorithm is specifically designed to estimate a distance between the generating models of the time series samples. The intuition for the Smash2.0 metric follows from a basic result in information theory: If we know the true distribution p of the random variable, we could construct a code with average description length $H(p)$, where $H(\cdot)$ is the entropy of a distribution. If, instead, we used the code for a distribution q , we would need $H(p) + D(p||q)$ bits on the average to describe the random variable. Thus, deviation in the distributions show up as KL divergence. If we can generalize the notion of KL divergence to processes, then it might be possible to quantify deviations in process dynamics via an increase in the entropy rate by the corresponding divergence.

Our ultimate goal is to design an algorithm that operates on a pair of data streams taking values in a finite data set. Nevertheless, to establish the correctness of our algorithm, we need to decide on a specific scheme for representing stochastic processes taking values in a finite alphabet. We further assume that our processes are ergodic and stationary. The specific modeling paradigm for modeling stochastic processes we use in this paper is called Probabilistic Finite-State Automaton, or PFSA for short, which has been studied in [9], [12], [4], [2]. PFSA model discrete value stochastic processes, and are strictly more expressive than Markov chain in the sense that it can generate processes that are not Markov of finite order[7]. It is also shown in [12] to be able to approximate any HMM with arbitrary accuracy. Moreover, PFSA has the property that many key statistical quantities of the processes they generate, such as entropy rate[8] and KL-divergence[19], enjoy closed-form formula, which are generally missing for more complicated models. The structural simplicity of PFSA combined with the clarity of its mathematical theory greatly facilitates the construction of efficient inference algorithms and its application as the underlying models to data mining and machine learning tasks with sequential data. Here we want to point out the resemblance of the PFSA model to the variational autoencoder (VAE) [25], [16] framework. The inference of PFSA from the

input can be thought as the training of the encoder in a VAE, and the performance of both the VAE and the PFSA model could be then evaluated by the log-likelihood of input as begin generated by the PFSA, as detailed in Sec. 2.2, or the decoder of the VAE.

One distance metric that is in the line of construction and exactly where Smash2.0 derives its name from is the *Smash* proposed in [4]. *Smash* is also based on PFSA modeling and designed directly to represent the difference or similarity between the *generating models of the sequences* rather than the sample path themselves. However, as while as both *Smash* and *Smash2.0* enjoy the advantage of not requiring dimensionality reduction or domain knowledge for feature extraction, *Smash2.0* is much more computationally efficient than *Smash*. In Sec. 6.3, we compare explicitly *Smash2.0* to two other distance metrics, *Smash* and *fastDTW*, a distance metric proposed in [26] that enjoys growing popularity. We show with a simple synthetic dataset that *Smash2.0* can surpass the other two algorithms at both computational efficiency and performance.

The remaining of the paper is organized as follows. In Sec. 2, we introduce basic concepts of stochastic processes and establish the correspondence between processes and labeled directed graphs via the core concept of causal state. The definition and basic properties of PFSA are introduced by the end of Sec. 2.2. In Sec. 3, with an in-depth study of the set of causal states, we answer the question of when will a stochastic process has a PFSA generator. An inference algorithm, *GenESeSs*, of PFSA is given in Sec. 4. We introduce the concept of reducedness of PFSA in Sec. 5.1, and the closed form formula for entropy rate and KL divergence of the processes generated by reduced PFSA are given in Sec. 5.2, together with theorem on log-likelihood convergence which is the key in learning with PFSA. In Sec. 6 we introduce the definition of 2.0 together with quantization of continuous sequences and the quality measurement of quantization scheme. We also compare *Smash2.0* with *Smash* and *fastDTW* in efficiency and performance at end of this section. In Sec. 7, we apply the distance metric proposed to two datasets arising from real world problems.

2 FOUNDATION

2.1 Stochastic Processes and Causal States

In this paper we study the generative model for stationary ergodic stochastic processes [22], [9] over a finite alphabet. Specifically, we consider a set of Σ -valued random variables $\{X_t\}_{t \in \mathbb{N}^+}$ indexed by positive integers representing time steps. By stationary, we mean strictly stationary, *i.e.* the finite-dimensional distributions[10] are invariant of time. By ergodic, we mean that all finite-dimensional distributions can be approximated with arbitrary accuracy with long enough realization. We are especially interested in processes in which the X_t s are *not* independent.

We denote the alphabet by Σ and use lower case Greeks (e.g. σ or τ) for symbols in Σ . We use lower case Latins (e.g. x or y) to denote sequences of symbols, $x = \sigma_1 \sigma_2 \dots \sigma_n$ for example, with the empty sequence denoted by λ . The length of a sequence x is denoted by $|x|$. The set of sequences of length d is denoted by Σ^d , and the collection of sequences of finite length is denoted by Σ^* , *i.e.* $\Sigma^* = \bigcup_{d=0}^{\infty} \Sigma^d$. We use Σ^ω to denote the set of infinitely long sequences, and $x\Sigma^\omega$ to denote the collection of infinite sequences with $x \in \Sigma^*$ as prefix. We note that, since all sequences can be viewed as prefixed by λ , we have $\lambda\Sigma^\omega = \Sigma^\omega$.

We note that $\mathcal{S} = \{x\Sigma^\omega \mid x \in \Sigma^*\}$ is a semiring over Σ^ω . Let $Pr(X_1 \dots X_n = \sigma_1 \dots \sigma_n)$ denote the probability of the process

producing a realization with $X_i = \sigma_i$ for $i = 1, \dots, n$, it is straightforward to verify that $\mu : \mathcal{S} \rightarrow [0, 1]$ defined by

$$\mu(\sigma_1 \dots \sigma_n \Sigma^\omega) = Pr(X_1 \dots X_n = \sigma_1 \dots \sigma_n), \quad (1)$$

is a premeasure on \mathcal{S} . By Charathéodory extension theorem, the σ -finite premeasure μ can be extended uniquely to a measure over $\mathcal{F} = \sigma(\mathcal{S})$, where $\sigma(\mathcal{S})$ is the σ -field generated by \mathcal{S} . Denoting the measure also by μ , we see that every stochastic process induces a probability space $(\Sigma^\omega, \mathcal{F}, \mu)$ over Σ^ω . In light of Eq. (1) and also for notational brevity, we denote $\mu(x\Sigma^\omega)$ by $Pr(x)$ when no confusion arises. We note that $Pr(\lambda) = \mu(\lambda\Sigma^\omega) = \mu(\Sigma^\omega) = 1$. Readers who are not familiar with the measure-theoretic terms used here can read Chap. 1 of [17] for reference.

Taking one step further, and denoting the collection of all measures over $(\Sigma^\omega, \mathcal{F})$ by \mathcal{M}_Σ , we see that we can get a family of measures in \mathcal{M}_Σ from a process in addition to μ .

Definition 1 (Observation Induced Measures). For $x \in \Sigma^*$ with $Pr(x) > 0$, the measure μ_x is the extension to \mathcal{F} of the premeasure defined on the semiring \mathcal{S} given by

$$\mu_x(y\Sigma^\omega) = \frac{Pr(xy)}{Pr(x)},$$

for all $y \in \Sigma^*$.

Now we introduce the concept of Probabilistic Nerode Equivalence, which was first introduced in [5].

Definition 2 (Probabilistic Nerode Equivalence). For any pair of sequences $x, y \in \Sigma^*$, x is equivalent to y , written as $x \sim y$, if and only if either $Pr(x) = Pr(y) = 0$, or $\mu_x = \mu_y$.

The interested reader can verify that the relation defined above is indeed an equivalence relation which is also *right-invariant* in the sense that $x \sim y \Rightarrow xz \sim yz$, for all $z \in \Sigma^*$. We denote the equivalence class of sequence x by $[x]$. We note that $\mu_{[x]}$ is well-defined because $\mu_x = \mu_y$ for $x, y \in [x]$. An equivalence class is also called a **causal state** [4] since the distribution of future events preceded by possibly distinct $x, y \in [x]$ are both determined by $\mu_{[x]}$. We denote $\mu_{[x]}(y\Sigma^\omega)$ by $Pr_{[x]}(y)$ when no confusion arises. We note that $\mu_{[\lambda]} = \mu$.

Remark 1. Since the equivalence class $\{x \in \Sigma^* \mid Pr(x) = 0\}$ plays no role in our future discussion, we ignore it as a causal state from this point on.

Definition 3 (Derivatives). For any $d \in \mathbb{N}^+$, the **d -th order derivative** of an equivalence class $[x]$, written as $\phi_{[x]}^d$, is defined to be the marginal distribution of $\mu_{[x]}$ on Σ^d , with the entry indexed by y denoted by $\phi_{[x]}^d(y)$. The first-order derivative is also called the **symbolic derivative**, in [4] since $\Sigma^1 = \Sigma$, and is denoted by $\phi_{[x]}$ for short. The derivative of a sequence is that of its equivalence class, *i.e.* $\phi_x^d = \phi_{[x]}^d$. We note that ϕ_x^d is the marginal distribution of μ on Σ^d , and is denoted by ϕ^d for short.

2.2 From Causal States to Probabilistic Automaton

From now on, we denote the set of causal states of a process by Q when no confusion arises. We start this section by showing that there is a labeled directed graph [1] associated with any stochastic process.

For any $q \in Q$ and $\sigma \in \Sigma$ such that $Pr_q(\sigma) > 0$, by right-invariance of probabilistic Nerode equivalence, there exists a $q' \in Q$, such that $x\sigma \in q'$ for all $x \in q$. Whenever the scenario described happens, we can put a directed edge from q to q' and label it by σ and $Pr_q(\sigma)$, and by doing this for all $q \in Q$ and

TABLE 1: Causality table of an order-1 Markov process with causal states $Q = \{q_\lambda, q_0, q_1\}$

x	$Pr(x)$	ϕ_x	causal state
λ	1	(.5, .5)	q_λ
0	.5	(.6, .4)	q_0
1	.5	(.4, .6)	q_1
00	.3	(.6, .4)	q_0
01	.2	(.4, .6)	q_1
10	.2	(.6, .4)	q_0
11	.3	(.4, .6)	q_1
000	.18	(.6, .4)	q_0
001	.12	(.4, .6)	q_1
010	.08	(.6, .4)	q_0
011	.12	(.4, .6)	q_1
100	.12	(.6, .4)	q_0
101	.08	(.4, .6)	q_1
110	.12	(.6, .4)	q_0
111	.18	(.4, .6)	q_1
\vdots	\vdots	\vdots	\vdots

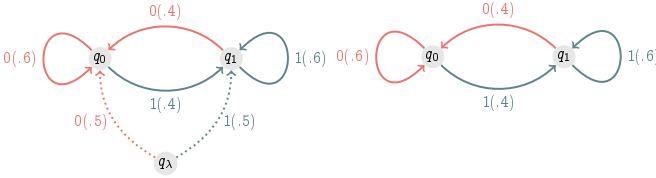


Fig. 1: The graph on left is the labeled directed graph constructed from Tab. 1. We note that the graph is *not* strongly connected since q_λ does not have any incoming edge. The graph on right is the strongly connected component of the graph on left.

$\sigma \in \Sigma$, we get a (possibly infinite) labeled directed graph with vertex set Q .

Example 1 (An Order-One Markov Process). We now carry out the construction described above on an order-1 Markov process [13] over alphabet $\Sigma = \{0, 1\}$, in which X_{t+1} follows a Bernoulli distribution conditioned on the value of X_t . Specifically we have

$$Pr(X_{t+1} = 0|X_t = 0) = .6, \quad Pr(X_{t+1} = 0|X_t = 1) = .4.$$

Together with the specification $Pr(X_1 = 0) = .5$, we can check that the process is stationary and ergodic. The reason that we choose this process as our first example is because it has a small set of causal states of size 3. We list the causal states of sequence up to length 3 in Tab. 1.

Since it is impossible to write down the infinite-dimensional distribution μ_x , we only show the symbolic derivative ϕ_x in Tab. 1, but we can verify that $\mu_x = \mu_y$ if and only if $\phi_x = \phi_y$ for this process.

Now, we conceptualize the labeled directed graph obtained from analyzing the causal states by an automaton structure[29], which we call probabilistic finite-state automaton[4], and show how we can get a stochastic process from it.

Definition 4 (Probabilistic Finite-State Automaton (PFSA)). A **probabilistic finite-state automaton** G is specified by a quadruple $(\Sigma, Q, \delta, \tilde{\pi})$, where Σ is a finite alphabet, Q is a finite set of states, δ is a partial map from $Q \times \Sigma$ to Q called transition map, and $\tilde{\pi}$, called observation probability, is a map from Q to \mathbf{P}_Σ , where \mathbf{P}_Σ is the space of probability distributions over Σ . The entry indexed by σ of $\tilde{\pi}(q)$ is written as $\tilde{\pi}(q, \sigma)$.

We call the directed graph (not necessarily simple with possible loops and multiedges) with vertices in Q and edges specified

by δ the **graph of the PFSA** and, unless stated otherwise, we assume it to be **strongly connected**[1], which means for any pair $q, q' \in Q$, there is a sequence $\sigma_1 \sigma_2 \cdots \sigma_k$, such that $\delta(q_{i-1}, \sigma_i) = q_i$ for $i = 1, 2, \dots, k$ with $q_0 = q$ and $q_k = q'$.

To generate a sequence of symbols, assuming G 's current state is q , it then outputs symbol σ with probability $\tilde{\pi}(q, \sigma)$, and moves to state $\delta(q, \sigma)$. We see that δ is partial because $\delta(q, \sigma)$ is undefined when $\tilde{\pi}(q, \sigma) = 0$.

Definition 5 (Observation and Transition Matrices). Given a PFSA $(\Sigma, Q, \delta, \tilde{\pi})$, the **observation matrix** $\tilde{\Pi}$ is the $|Q| \times |\Sigma|$ matrix with the (q, σ) -entry given by $\tilde{\pi}(q, \sigma)$, and the **transition matrix** Π is the $|Q| \times |Q|$ matrix with the (q, q') -entry $\pi(q, q')$, given by

$$\pi(q, q') = \sum_{\{\sigma: \delta(q, \sigma) = q'\}} \tilde{\pi}(q, \sigma).$$

It is straightforward to verify that both Π and $\tilde{\Pi}$ are stochastic, *i.e.* nonnegative with rows of sum 1.

Remark 2. We borrow the terms *observation matrix* and *transition matrix* from the study of HMM [28]. However, we need to point out here that our model differs from the HMM in that, in HMM, the transition from the current state to the next one is independent of the symbol generated by the current state, while in PFSA, the current state and symbol generated together determine the next state the PFSA will be in as specified by the transition map δ .

The interested reader might have noticed that we haven't specified the initial distribution on states for the process to start with. The reason is that, unless specified otherwise, we assume the initial distribution to be the **stationary distribution**[15] of Π . We denote the stationary distribution of G by \mathbf{p}_G , or by \mathbf{p} if G is understood.

Theorem 1 (PFSA Generates Stationary Ergodic Processes). *Stochastic process generated by a PFSA G with distribution on states initialized with \mathbf{p}_G is stationary and ergodic.*

proof omitted. Example 1 shows that we may derive a PFSA from a stationary ergodic process, and Thm. 1 shows that the process generated by the PFSA thus obtained is also stationary and ergodic. This motivates us to seek a characterization for stochastic processes that gives rise to a PFSA. Since the process in Example 1 is an order-1 Markov process, which is the simplest non-i.i.d. process, it is legitimate to ask whether a process has to be Markov to have a PFSA generator. This desired characterization may be obtained from analyzing the notion of causal states, which we investigate in the next section.

Remark 3. Table 2 compares the three generative models of stochastic processes mentioned above: Markov chain(MC), PFSA, and hidden Markov model(HMM). We note that a Markov chain produces a sequence of states, while sequences produced by PFSA and hidden Markov model take values in their respect output alphabets. We can also see that HMM can be considered as an extension to MC by adding an output alphabet and observation probabilities (in blue in the following example). Quite clearly, PFSAs are not directly comparable to either MC or HMM.

3 STOCHASTIC PROCESSES WITH PFSA GENERATOR

3.1 Persistent Causal States

Definition 6 (Persistent and Transient Causal States). Let Q be the set of causal states of a stationary ergodic process. For every $q \in Q$ and $d \in \mathbb{N}$, let $p_d(q) = \phi^d \{[x] = q\}$, *i.e.* the probability of length- d sequences who are equivalent to q . A causal state q is

TABLE 2: Comparing Markov chain, PFSA, and hidden Markov model.

Model	Defining variables	Example
MC	Set of states; Transition probabilities.	
PFSA	Set of states; Output alphabet; Transition function; Observation probabilities.	
HMM	Set of states; Output alphabet; Transition probabilities; Observation probabilities.	

persistent if $\liminf_{d \rightarrow \infty} p_d(q) > 0$, and **transient** if otherwise. We denote the subset of all persistent causal states by Q^+ .

Remark 4. Here we borrow the term *transient state* from the study of Markov chains, but we should note that the two concepts are not identical. For an introduction to Markov chain, we refer the interested reader to [13]. A Markov chain never revisits transient states as soon it hits a recurrent state. However, although a transient causal state could be like a transient state of a Markov chain, as the q_λ in Example 1, it could also be revisited for infinitely many times, as a recurrent state of a Markov chain does. The reason we borrow the term is because the concepts are also similar in an important aspect: The probability a Markov chain being in a transient state diminishes as time increases, and a transient causal states also has $\liminf_{d \rightarrow \infty} p_d(q) = 0$. Since transient causal states can recur, we coin the name persistent causal states for the counterpart of transient causal states instead of borrowing the recurrent state also from Markov chain.

For any pair $q, q' \in Q$, let $\pi_{q,q'} = \sum_{\{\sigma: q\sigma = q'\}} \phi_q(\sigma)$, where the expression $q\sigma = q'$ is a shorthand for $[x\sigma] = q'$ for all $[x] = q$. The following proposition shows that $\pi_{q,q'}$ captures the flow of probability over causal states as sequence length increases.

Proposition 1. We have $p_d(q') = \sum_{q \in Q} \pi_{q,q'} p_{d-1}(q)$ for each $q' \in Q$ and $d \in \mathbb{N}^+$. Furthermore, there is no flow from a persistent state to a transient one, i.e. $\pi_{q,q'} = 0$ for $q \in Q^+$ and $q' \in Q \setminus Q^+$.

proof omitted.

Theorem 2. Let Q^+ be the set of persistent causal states of a stationary ergodic process \mathcal{P} . Then, $p(q) = \lim_{d \rightarrow \infty} p_d(q)$ exists for every $q \in Q^+$. Furthermore, if Q^+ is finite and $\sum_{q \in Q^+} p(q) = 1$, the process generated by the PFSA $G = (\Sigma, Q^+, \delta, \tilde{\pi})$ with $\delta(q, \sigma) = q\sigma$ and $\tilde{\pi}(q, \sigma) = \phi_q(\sigma)$ is exactly \mathcal{P} . In fact, we have $p_G|_q = p(q)$ for $q \in Q^+$.

proof omitted.

Example 2 (An Order-Two Markov Process). Now, let us consider an order-2 Markov process over alphabet $\Sigma = \{0, 1\}$, in which X_{t+2} follows a Bernoulli distribution conditioned on the value of $X_t X_{t+1}$. More specifically, denoting $\Pr(X_{t+2} = 0 | X_t X_{t+1} = ij)$ by p_{ij} for $i, j \in \{0, 1\}$, we have

TABLE 3: Causality table of an order-2 Markov process with causal states $Q = \{q_\lambda, q_0, q_1, q_{00}, q_{01}, q_{10}, q_{11}\}$. The reader can see that the causal states q_{00}, q_{01}, q_{10} , and q_{11} are named after the last two symbols of the corresponding sequences, which is a demonstration of the order-2 Markovity of the process, i.e. the distribution of future events is determined completely by length-2 immediate history.

x	$Pr(x)$	ϕ_x	causal state
λ	1	$(1/2, 1/2)$	q_λ
0	$1/2$	$(8/15, 7/15)$	q_0
1	$1/2$	$(7/15, 8/15)$	q_1
00	$4/15$	$(3/10, 7/10)$	q_{00}
01	$7/30$	$(1/5, 4/5)$	q_{01}
10	$7/30$	$(4/5, 1/5)$	q_{10}
11	$4/15$	$(7/10, 3/10)$	q_{11}
000	$2/25$	$(3/10, 7/10)$	q_{00}
001	$14/75$	$(1/5, 4/5)$	q_{01}
010	$7/150$	$(4/5, 1/5)$	q_{10}
011	$14/75$	$(7/10, 3/10)$	q_{11}
100	$14/75$	$3/10, 7/10$	q_{00}
101	$7/150$	$(1/5, 4/5)$	q_{01}
110	$14/75$	$(4/5, 1/5)$	q_{10}
111	$2/25$	$(7/10, 3/10)$	q_{11}
:	:	:	:

$p_{00} = .3, p_{01} = .2, p_{10} = .8, p_{11} = .7$. Together with the specification $\Pr(X_2 = 0 | X_1 = 0) = 8/15, \Pr(X_2 = 0 | X_1 = 1) = 7/15$, and $\Pr(X_1 = 0) = .5$, we can check that the process is stationary and ergodic. We list the causal states of sequence up to length 3 in Tab. 3.

Since it is impossible to write down the infinite-dimensional distribution μ_x , we only show ϕ_x in Tab. 3, but we can check that $\phi_x = \phi_y$ if and only if $\mu_x = \mu_y$ for this process. Since q_λ, q_0, q_1 only show up once, while $q_{00}, q_{01}, q_{10}, q_{11}$ appear repeatedly, we have $Q^+ = \{q_{00}, q_{01}, q_{10}, q_{11}\}$. With more detailed calculation, we can show that $p(q_{00}) = 4/15, p(q_{01}) = 7/30, p(q_{10}) = 7/30$, and $p(q_{11}) = 4/15$, which sum up to 1. According to Thm. 2, we can construct a PFSA with state set Q^+ that generates exactly the same process. We demonstrate the labeled directed graph constructed on Q in Fig. 2, and the PFSA is exactly the induced subgraph[24] on Q^+ , which is also the unique strongly connected component of the graph. We can show that the stationary distribution of the PFSA is exactly $(4/15, 7/30, 7/30, 4/15)$.

Example 3 (A PFSA on Three States). In this example, we analyze the stochastic process generated by the PFSA on the left of Fig. 3. We nickname the PFSA as T . We show that Q of this process is infinite, while Q^+ is of size 3. We first notice that, no matter what state the PFSA resides, the sequence 11, and hence any sequence ending in 11, will take it to state r , which generates symbol 0 with probability .8, and 1 with probability .2. We also note that, whenever there are two consecutive 1s in a given sequence in Σ^* , we know for sure the state the PFSA resides. For example, sequence 110 will take the PFSA to s , and 1101, to q . On the left of Fig. 4, we show the probabilities of causal states [11], [110], [1101], and the sum of probabilities of all other causal states for sequence length $d = 0, \dots, 25$. We see from the bar plots that the sum of concentrations of [11], [110], and [1101] approaches 1 as d increases. We also point out that, with all numbers rounded up to three decimal places, $p_{25}([11]) = 0.182, p_{25}([110]) = 0.474$, and $p_{25}([1101]) = 0.279$, while the stationary distributions of the states r, s , and q are 0.190, 0.506, 0.304, respectively.

However, we also note that Q of the process is actually infinite by observing the fact that $\phi_{[0^d]}$, where σ^d means σ repeated d

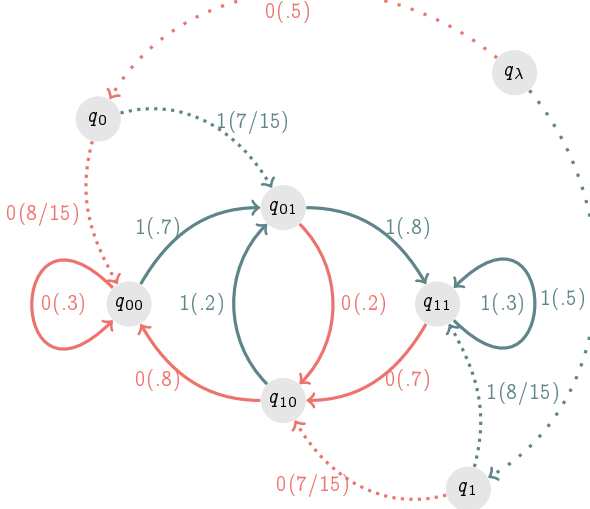


Fig. 2: Labeled directed graph obtained from Tab. 3. The edges from transient causal states are dotted, while those from persistent states are solid.

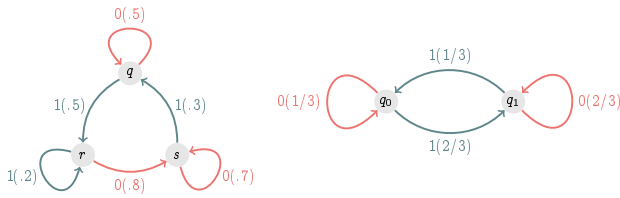


Fig. 3: The PFSA T on left generates a stochastic process with infinite Q and Q^+ of size 3. The PFSA S on right generates a stochastic process with empty Q^+ but \overline{Q}^+ (defined in Sec. 3.2) of size 2.

times, are all distinctive.

We note that the process generated by this PFSA is *not* Markov, as implied by the infinity of Q . However, the fact that there are only three persistent causal states whose sum of probabilities approaches 1 allows it to have a PFSA generator.

Example 4 (A Stochastic Process with Empty Q^+). In this example, we analyze the stochastic process generated by the PFSA on the left of Fig. 3. We nickname the PFSA as S . We show that Q of this process is infinite while Q^+ is empty. Without run into details of the computation, we point out the fact that causal states of this process are also uniquely characterized by their symbolic derivatives, and the set $\{\phi(q) | q \in Q\}$ is in one-to-one correspondence with \mathbb{Z} . More specifically, we have

$$Q = \{q_n \mid \phi_{q_n} \propto (.5^{n+1} + 1, .5^n + .5), n \in \mathbb{Z}\}, \quad (2)$$

where \propto means being proportional to, and

$$\pi_{q_n, q_{n+1}} = \frac{2 \cdot .5^{n+1} + 1}{3 \cdot .5^n + 1}, \quad \pi_{q_n, q_{-n+1}} = \frac{1 \cdot .5^{n-1} + 1}{3 \cdot .5^n + 1},$$

with $\pi_{q_n, q_{n+1}} + \pi_{q_n, q_{-n+1}} = 1$, for all $n \in \mathbb{Z}$. We demonstrate on the left of Fig. 4 the contour of $p_d(q_n)$ against n for sequence length $d = 10, 20, \dots, 150$. It takes some more work to show rigorously, but we can speculate that, for any fixed $n \in \mathbb{Z}$, $p_d(q_n)$ approaches 0 as d approaches infinity, as the curves flatten out with increasing d .

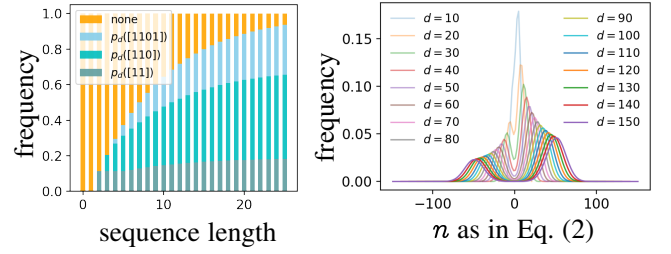


Fig. 4: The bar plot on left shows the probabilities of [11], [110], and [1101] for sequence length $d = 0, 1, \dots, 25$ as discussed in Example 3. The curves on right show the contour of $p_d(q_n)$ against n for sequence length $d = 10, 20, \dots, 150$ as discussed in Example 4.

3.2 Accumulation Causal States

We see from Example 4 that we can have a PFSA that generates stochastic process with empty Q^+ . In such a case, can we still get the PFSA structure back by studying the the set of causal states of the process? The answer is yes.

Definition 7 (Epsilon-Ball of Measure). Denote the collection all measures on $(\Sigma^\omega, \mathcal{F})$ by \mathcal{M}_Σ , and let $\nu \in \mathcal{M}_\Sigma$, the ε -ball of order d centered at ν is defined by

$$B_{d,\varepsilon}(\nu) = \left\{ \nu' \in \mathcal{M}_\Sigma \mid \sum_{x \in \Sigma^d} |\nu'(x\Sigma^\omega) - \nu(x\Sigma^\omega)| < \varepsilon \right\}.$$

In another words, $B_{d,\varepsilon}$ is the collection of all measures that is no more than ε away from ν with respect to total variation distance over Σ^d .

Definition 8 (Accumulation Causal States). Let Q be the set of causal states of a stochastic process \mathcal{P} , a measure $\nu \in \mathcal{M}_\Sigma$ is an **accumulation causal state** of \mathcal{P} if

$$p_{l,d,\varepsilon}(\nu) = \phi^l \{ \mu_{[x]} \in B_{d,\varepsilon}(\nu) \}$$

satisfies $p_{d,\varepsilon}(\nu) = \liminf_{l \rightarrow \infty} p_{l,d,\varepsilon}(\nu) > 0$ for all $d \in \mathbb{N}^+$ and $\varepsilon > 0$. That is, a measure ν is accumulation causal state if, no matter how large d is and how small ε is, the sum of probabilities of length- l sequences falling in $B_{d,\varepsilon}(\nu)$ does not vanish as l approaches infinity.

The collection of accumulation causal states is denoted by \overline{Q} . Since $p_{d,\varepsilon}(\nu)$ is monotonically decreasing as $d \rightarrow \infty$ and $\varepsilon \rightarrow 0$, $p(\nu) = \lim_{d \rightarrow \infty} \lim_{\varepsilon \rightarrow 0} p_{d,\varepsilon}(\nu)$ is well-defined. A measure ν with $p(\nu) > 0$ is called an **atomic accumulation causal state**, and the collection of all atomic accumulation causal states is denoted by \overline{Q}^+ .

Definition 9 (Translation Measure). Let $\nu \in \mathcal{M}_\Sigma$, the translation of ν by σ for $\nu(\sigma\Sigma^\omega) > 0$, denoted by ν_σ , is the extension to \mathcal{F} of the premeasure on the semiring \mathcal{S} given by

$$\nu_\sigma(x\Sigma^\omega) = \frac{\nu(\sigma x\Sigma^\omega)}{\nu(\sigma\Sigma^\omega)}.$$

Proposition 2. \overline{Q}^+ is closed under translation.
proof omitted.

Theorem 3. Let \mathcal{P} be a stationary ergodic stochastic process with finite \overline{Q}^+ and $\sum_{\nu \in \overline{Q}^+} p(\nu) = 1$. Then the process generated by the PFSA $G = (\Sigma, \overline{Q}^+, \delta, \tilde{\pi})$ with $\delta(\nu, \sigma) = \nu_\sigma$ and $\tilde{\pi}(\nu, \sigma) = \nu(\sigma\Sigma^\omega)$ is exactly \mathcal{P} . In fact, we have $\mathbf{p}_G|_\nu = p(\nu)$.

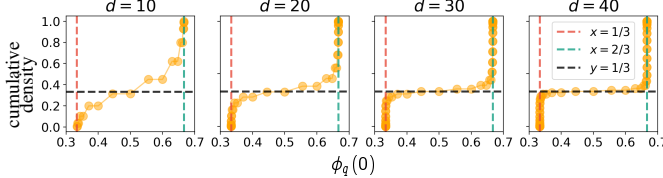


Fig. 5: Cumulative probability density function of $\phi_q(0)$.

proof omitted.

Example 5 (Example 4 Revisited). We demonstrate that \overline{Q}^+ of the process in Example 4 has two elements, again by observation. We plot the cumulative probability density functions of $\phi_q(0)$ for each sequence length $d = 10, 20, 30, 40$ in Fig. 5. More specifically, for each fixed d , the x -coordinates of the dots are in $\Phi^d = \{\phi_{[x]}(0) \mid x \in \Sigma^d\}$, while the y -coordinate of a dot with x -coordinate $h_0 \in \Phi^d$ equals $\phi^d(\{\phi_{[x]}(0) \leq h_0\})$. We can see clearly that, the cumulative function converges to a step function with steps at $1/3$ and $2/3$ as d increases. The fact implies that $\nu \in \overline{Q}^+$ satisfies that $\nu(0\Sigma^\omega)$ is either $1/3$ or $2/3$. We see from (2) that the two measures in \overline{Q}^+ are exactly q_∞ and q_∞ . Fig. 5 also implies that that $p(q_\infty) = 1/3$ and $p(q_\infty) = 2/3$, which is exactly the stationary distribution on the state set of the PFSA.

4 INFERENCE ALGORITHM OF PFSA

From the discussion in Sec. 3, we see that a stochastic process enjoys an PFSA generator if either finitely many causal states get all the probability in the limit, as described in Sec. 3.1, or there exists finitely many measures in \mathcal{M}_Σ whose arbitrarily small neighborhoods are going to be populated by all the causal states in the limit, as described in Sec. 3.2. The implications of these observation goes beyond a theoretical development of PFSA, but also guide us through the designing of inference algorithms of the model. In fact, a valid heuristic of the inference algorithm of PFSA would be to apply any clustering algorithm to the set of causal states corresponding to sequences up to a certain length, and use the center of the clusters to serve as estimates to the states. However, this primitive heuristic has a drawback since the cluster structure of $\{[x] \mid x \in \Sigma^d\}$ may not be clear enough to facilitate a clustering algorithm. In order to get better estimates of the states, we need something to fine tune our view into the set of causal states, which we call ε -synchronizing sequence[2].

4.1 Epsilon-synchronizing Sequences

Before introducing ε -synchronizing sequence, we first introduce the concept of observation induced distributions over the state set. Let G be a PFSA, we know that the initial distribution over states is exactly the stationary distribution \mathbf{p}_G . Let us assume that the first symbol generated by G is σ , denote by $\mathbf{p}_G(\sigma)$ the distribution over states after G producing σ , we have

$$\mathbf{p}_G(\sigma)|_q = \frac{1}{Z} \sum_{\{q' \mid \delta(q', \sigma) = q\}} \tilde{\pi}(q', \sigma) \mathbf{p}_G|_{q'},$$

where

$$Z = \sum_{q \in Q} \sum_{\{q' \mid \delta(q', \sigma) = q\}} \tilde{\pi}(q', \sigma) \mathbf{p}_G|_{q'},$$

is the normalizer.

Definition 10 (Observation induced distributions). Let $x = \sigma_1 \dots \sigma_n$ be a sequence observed, the distribution over states induced by x is defined inductively by

$$\mathbf{p}_G(\sigma_1 \dots \sigma_i)|_q = \frac{1}{Z} \sum_{\{q' \mid \delta(q', \sigma_i) = q\}} \tilde{\pi}(q', \sigma) \mathbf{p}_G(\sigma_1 \dots \sigma_{i-1})|_{q'},$$

where

$$Z = \sum_{q \in Q} \sum_{\{q' \mid \delta(q', \sigma_i) = q\}} \tilde{\pi}(q', \sigma) \mathbf{p}_G(\sigma_1 \dots \sigma_{i-1})|_{q'},$$

for $i = 1, \dots, n$, with the base case $\mathbf{p}_G(\lambda) = \mathbf{p}_G$.

Definition 11 (ε -synchronizing sequence). Let G be a strongly connected PFSA on state set Q and over alphabet Σ . A sequence $x \in \Sigma^*$ is called an **ε -synchronizing sequence** for some $\varepsilon > 0$ if there exists a $q \in Q$ such that $\|\mathbf{p}_G(x) - \mathbf{e}_q\|_\infty < \varepsilon$, where \mathbf{e}_q is the base probability vector with the entry indexed by q equalling 1.

Without running into details, we want to point out here that the concept of ε -synchronizing sequence is the center piece for the theoretic development of PFSA, including the formula for entropy rate and KL divergence, which we are going to discuss in Sec. 5. Although we omit the proofs in this paper and hence wouldn't see ε -synchronizing sequences in real play of proving theorems, we will soon see its role in PFSA inference algorithm, and the reason the ε -synchronizing sequences are important to inference is because that $\{[x_\varepsilon x] \mid x \in \Sigma^d\}$ tends to have a much clearer cluster structure than $\{[x] \mid x \in \Sigma^d\}$ for an ε -synchronizing sequence x_ε .

4.2 GenESeSs Algorithm

We give a brief review to the algorithm called GenESeSs proposed in [3] in this section. By a sub-sequence, we mean a consecutive sub-sequence.

Definition 12 (Empirical Symbolic Derivative). Let $x \in \Sigma^*$, the empirical symbolic derivative $\hat{\phi}_y^x$ of a sub-sequence y of x is given by

$$\hat{\phi}_y^x(\sigma) = \frac{\text{number of sub-sequence } y\sigma \text{ in } x}{\text{number of sub-sequence } y \text{ in } x},$$

for all $\sigma \in \Sigma$.

Our inference algorithm is called GenESeSs for Generator Extraction Using Self-similar Semantics, With the input of a long enough observed sequence x , GenESeSs takes the following three steps to infer a PFSA:

Step one: Approximate ε -synchronizing sequence: Calculate

$$\mathcal{D}_\varepsilon^x = \left\{ \hat{\phi}_y^x \mid y \text{ is a sub-sequence of } x \text{ with } |y| \leq \log_{|\Sigma|} \frac{1}{\varepsilon} \right\},$$

Then, select a sequence x_ε with $\hat{\phi}_{x_\varepsilon}^x$ being a vertex of the convex hull of $\mathcal{D}_\varepsilon^x$.

Step Two: Identify transition structure: For each state q , we associate a sequence identifier $x_q \in x_\varepsilon \Sigma^*$, and a probability distribution d_q on Σ . We extend the structure recursively: Initialize the state set as $Q = \{q_0\}$, find x_{q_0} and set $d_{q_0} = \hat{\phi}_{x_{q_0}}^x$; Calculate the empirical symbolic derivative of $x_q \sigma$ for each state $q \in Q$ and $\sigma \in \Sigma$. If $\|\hat{\phi}_{x_q \sigma}^x - d_{q'}\|_\infty \leq \varepsilon$ for some $q' \in Q$, then define $\delta(q, \sigma) = q'$. However, if no such q' exists in Q , add a new state q' to Q , and define $x_{q'} = x_q \sigma$, and $d_{q'} = \hat{\phi}_{x_{q'} \sigma}^x$. The process terminates when no more states can be added to Q . The inferred PFSA is the strongly connected component of the directed graph thus obtained.

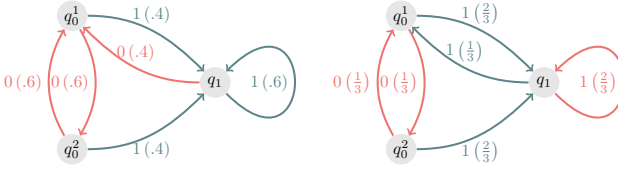


Fig. 6: Non-reduced PFSA.

Step Three: Identify observation probabilities: Initialize counter N_σ^q for each state q and symbol σ ; choose an arbitrary initial state in the graph obtained in step two and run sequence x through it, *i.e.* if current state is q , and the next symbol from x is σ , then move to $\delta(q, \sigma)$, and add 1 to counter N_σ^q ; finally, calculate the observation probability map by $\tilde{\pi}(q) = \left[(N_\sigma^q)_{\sigma \in \Sigma} \right]$.

5 ENTROPY RATE AND KL DIVERGENCE

5.1 Irreducibility of PFSA

We first discuss the concept of irreducibility for PFSA.

Definition 13. A PFSA G is irreducible if there no other PFSA with strictly fewer number of states that generate the same stochastic process as G does.

The definition of PFSA itself doesn't ensure irreducibility, as shown by the following example.

Example 6 (Non-reduced PFSA). Here we show two examples of a reducible PFSA. The PFSA on left generates the same process as the PFSA on the right Fig. 1 does, while the one on right generates the same process as the PFSA on the right of Fig. 3 does, but both with one more state.

Definition 14 (Measure of state μ_q and Equivalent States). Let a PFSA be specified by the quadruple $(\Sigma, Q, \delta, \tilde{\pi})$, the measure μ_q is defined by $\mu_q(x\Sigma^\omega) = \tilde{\pi}(q, x)$. Two states $q, q' \in Q$ are **equivalent** if and only $\mu_q = \mu_{q'}$.

We note that q_0^1 and q_0^2 in both PFSA in Fig. 6 are equivalent. We also see that we can get the reduced PFSA back by collapsing equivalent states to a single state.

Theorem 4 (Characterization of Irreducibility). A PFSA is irreducible if and only if it has no equivalent states. Furthermore, a reduced PFSA is unique, in the sense that, if two reduced PFSA $G_1 = (\Sigma, Q_1, \delta_1, \tilde{\pi}_1)$ and $G_2 = (\Sigma, Q_2, \delta_2, \tilde{\pi}_2)$ generate the same stochastic process, we must have there is a one-to-one correspondence between $f : Q_1 \rightarrow Q_2$ such that $\delta_1(q) = \delta_2(f(q))$.

Corollary 1. The PFSA constructed on the set of persistent states Q^+ and the set of atomic accumulation states \overline{Q}^+ are reduced.

5.2 Entropy Rate and KL Divergence

Definition 15 (Entropy rate and KL divergence). By entropy rate of a PFSA, we mean the entropy rate of the stochastic process generated by the PFSA[8]. Similarly, by KL divergence of two PFSA, we mean the KL divergence between the two processes generated by them [19]. More precisely, we have

$$\mathcal{H}(G) = -\lim_{d \rightarrow \infty} \frac{1}{d} \sum_{x \in \Sigma^d} \Pr(x) \log \Pr(x),$$

and the KL divergence

$$\mathcal{D}_{\text{KL}}(G \parallel H) = \lim_{d \rightarrow \infty} \frac{1}{d} \sum_{x \in \Sigma^d} \Pr_G(x) \log \frac{\Pr_G(x)}{\Pr_H(x)},$$

whenever the limits exist.

Theorem 5 (Closed-form Formula for Entropy Rate). The entropy rate of a PFSA $G = (\Sigma, Q, \delta, \tilde{\pi})$ is given by

$$\mathcal{H}(G) = \sum_{q \in Q} \Pr(q) \cdot h(\tilde{\pi}(q)),$$

where $h(\cdot)$ is the entropy of a probability distribution.
proof omitted.

Theorem 6 (Closed-form Formula for KL Divergence). Let $G = (\Sigma, Q, \delta, \tilde{\pi})$ and $G' = (\Sigma, Q', \delta', \tilde{\pi}')$ be two PFSA, and let $\Pr_G(q, q')$ be the joint G -probability of joint state (q, q') , then we have the KL divergence between the G and G' is given by

$$\sum_{(q, q') \in Q \times Q'} \Pr_G(q, q') D_{\text{KL}}(\tilde{\pi}(q) \parallel \tilde{\pi}'(q')),$$

where $D_{\text{KL}}(\cdot \parallel \cdot)$ is the KL divergence between two probability distributions.

proof omitted.

5.3 Log-likelihood

Definition 16 (Log-likelihood). Let $x \in \Sigma^d$, the log-likelihood [8] of a PFSA G generating x is given by

$$L(x, G) = -\frac{1}{d} \log \Pr_G(x)$$

Theorem 7 (Convergence of log-likelihood). Let G and H be two reduced PFSA, and let $x \in \Sigma^d$ be a sequence generated by G . Then we have

$$L(x, H) \rightarrow \mathcal{H}(G) + \mathcal{D}_{\text{KL}}(G \parallel H),$$

in probability as $d \rightarrow \infty$.

sketch of proof: We first notice that

$$\begin{aligned} & \sum_{x \in \Sigma^d} \Pr_G(x) \log \frac{\Pr_G(x)}{\Pr_{G'}(x)} \\ &= \sum_{x \in \Sigma^{d-1}} \sum_{\sigma \in \Sigma} \Pr_G(x) \Pr_G(x) \left. \tilde{\Pi}_G \right|_{\sigma} \log \frac{\Pr_G(x) \Pr_G(x) \left. \tilde{\Pi}_G \right|_{\sigma}}{\Pr_H(x) \Pr_H(x) \left. \tilde{\Pi}_H \right|_{\sigma}} \\ &= \sum_{x \in \Sigma^{d-1}} \Pr_G(x) \log \frac{\Pr_G(x)}{\Pr_H(x)} \\ &+ \underbrace{\sum_{x \in \Sigma^{d-1}} \Pr_G(x) \sum_{\sigma \in \Sigma} \Pr_G(x) \left. \tilde{\Pi}_G \right|_{\sigma} \log \frac{\Pr_G(x) \left. \tilde{\Pi}_G \right|_{\sigma}}{\Pr_H(x) \left. \tilde{\Pi}_H \right|_{\sigma}}}_{D^d}. \end{aligned}$$

By induction, we have $\mathcal{D}_{\text{KL}}(G \parallel H) = \lim_{d \rightarrow \infty} \frac{1}{d} \sum_{i=1}^d D^i$, and hence by Cesàro summation theorem, $\mathcal{D}_{\text{KL}}(G \parallel H) = \lim_{d \rightarrow \infty} D^d$.

Let $x = \sigma_1 \sigma_2 \dots \sigma_n$ be a sequence generated by G . Let $x^{[n-1]}$ is the truncation of x at the $(i-1)$ -th symbols, we have

$$\begin{aligned} & -\frac{1}{n} \sum_{i=1}^n \log \Pr_H(x^{[i-1]}) \left. \tilde{\Pi}_H \right|_{\sigma_i} \\ &= \underbrace{\frac{1}{n} \sum_{i=1}^n \log \frac{\Pr_G(x^{[i-1]}) \left. \tilde{\Pi}_G \right|_{\sigma_i}}{\Pr_H(x^{[i-1]}) \left. \tilde{\Pi}_H \right|_{\sigma_i}}}_{A_{x,n}} - \underbrace{\frac{1}{n} \sum_{i=1}^n \log \Pr_G(x^{[i-1]}) \left. \tilde{\Pi}_G \right|_{\sigma_i}}_{B_{x,n}}. \end{aligned}$$

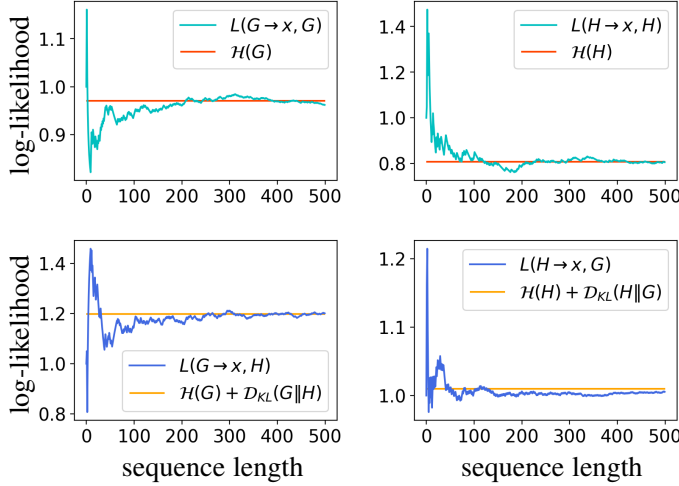


Fig. 7: Examples of log-likelihood convergence. We use a horizontal line to demonstrate the limit the log-likelihood should approach to as length of sequence increases.

Since the stochastic process G generates is ergodic, we have

$$\lim_{n \rightarrow \infty} A_{x,n} = \lim_{d \rightarrow \infty} D^d = \mathcal{D}_{\text{KL}}(G \parallel H),$$

and $\lim_{n \rightarrow \infty} B_{x,n} = \mathcal{H}(G)$. \square

Example 7. In this example we show the convergence of log-likelihood using the PFSA G on the left of Fig. 1 and the PFSA H that is the induced subgraph on q_{00}, q_{01}, q_{10} , and q_{11} in Fig. 2. We have

$$\mathcal{H}(G) \approx 0.9710, \quad \mathcal{H}(H) \approx 0.8069,$$

and

$$\mathcal{D}_{\text{KL}}(G \parallel H) \approx 0.2266, \quad \mathcal{D}_{\text{KL}}(H \parallel G) \approx 0.2030.$$

Let use $G \rightarrow x$ as the short hand for x is generated by G , we show in Fig. 7 the log-likelihood of G producing a sequence x generated by G (top left), the log-likelihood of H producing a sequence x generated by H (top right), the log-likelihood of H producing a sequence x generated by G (lower left), and the log-likelihood of G producing a sequence x generated by H (lower right). We can clearly see that the convergence of log-likelihood from the plots.

6 SMASH2.0

Because PFSA is a model for sequences on finite alphabet, continuous-valued sequences should first be quantized to discrete ones before we can model them directly with PFSA. However, here arises the question as to what constitutes a correct way of doing quantization. More often than not, the answer is not provided explicitly either by the dataset or the learning task at hand, and tends to be not unique, and the strategy we take to tackle the problem, as discussed briefly in Sec. 6.1, is to construct, not one, but a set of quantization schemes in the hope of exploring the dataset from more angles and to a fuller extent.

Now with the assumption of discrete input, we then show in Sec. 6.2 how the log-likelihood technique can help equip a set of sequences with a pairwise distance, with which all kinds of distance-based machine learning algorithms could then be carried out on the set. However, since the performance of such a machine

learning algorithm can depend on the quality of the distance metric heavily, and different quantization give different distance, we also need to have a way to evaluate the quality of a quantization scheme in term of the distance it induces. Such an evaluation is required both for testing the fitness of the model and for quality control should the distances be used as feed in a pipeline to later computation. We propose such an evaluation also in Sec. 6.2.

Finally we apply the techniques introduced above to two time series datasets, one with EEG recordings in Sec. 7.1 and one with sensor data in Sec. 7.2.

6.1 Quantization of Continuous Sequence

The simplest approach to turn a continuous sequence to a symbolic one with alphabet size k is by choosing $k-1$ cut-off points $p_1 < p_2 < \dots < p_{k-1}$. With the additional assumption that $p_0 = -\infty$ and $p_k = +\infty$, we can replace a data point p in the continuous sequence with symbol i if $p \in [p_i, p_{i+1})$. We call the set of cut-off points a *partition*. The most common practice of choosing a partition is to apply the entropy maximization principle, in which the p_i 's are chosen so that we have as equal as possible numbers of data points falling in each interval $[p_i, p_{i+1})$. However, we can also perturb the cut-off points a little bit so that the distribution of symbols in the quantized sequences have smaller entropy. In the numerical experiments below, we also try k -part partitions with one symbol i , $i = 1, \dots, k$, in the quantized sequences being more than the others, so that the entropy of the symbol distribution is at 90% percent of the maximum entropy.

The partition approach is efficient to carry out and empirically effective in many cases, however we can also foresee that such a simple quantization scheme may work sub-optimally in the following two scenarios: first, the input sequences share a common trend; second, the input sequences have shifts and re-scalings that are tangential to the property of the sequences we are interested in. An example of the first case is the stock prices dataset, and examples for the second case are common among datasets composed of voltage recordings that have different reference potentials or sound recordings that have different volumes. In order to fine-tune to the properties that make the real distinctions between sequences from different classes, We may want to first take derivatives (or detrend) and normalize the sequences to have empirical mean 0 and variance 1 before they are translated to symbolic sequences using a partition. We point out that even when there is no obvious trend in the sequence, the property of interest may still hide in the derivatives, in which case detrending is of great value.

In our study of PFSA modeling, we try to use as many different quantization schemes as possible in the hope of exploring the dataset to a fuller extent. We do so by combining different decisions for whether to detrend and normalize and different choice of partitions to form a pool of quantization schemes. To record the parameters for a quantization scheme, we develop the following shorthand: 1) Dd, with d being a non-negative integer, means detrending d times; 2) N0 means not to apply normalization, and N1, apply normalization; 3) $[p_1 \ p_2 \ \dots \ p_{k-1}]$ means a k -part partition with cut-off points p_i 's. As an example, D1N1[3.] means that we first detrend once, then normalize, and finally all data points in the resulting sequence that are less than 3. is replaced with a symbol 0, and those greater than or equal to 3., symbol 1.

6.2 SMASH2.0: Distance between Time Series

The way we calculate distance between two sequences is as follows. We first choose a set of PFSA $\mathcal{G} = \{G_1, \dots, G_k\}$ as

base, and the coordinate for a sequence \mathbf{x} is defined to be

$$(L(\mathbf{x}, G_1), \dots, L(\mathbf{x}, G_k)),$$

where $L(\mathbf{x}, G)$ is the log-likelihood of G generating \mathbf{x} , as defined in detail in Sec. 5. The distance between a pair of sequences can then be any valid distance between their coordinates.

For example, for the two numerical experiments in Sec. 7, we use \mathcal{G} that contains four PFSA

1. $\delta(q_0, 0) = q_0, \delta(q_0, 1) = q_1, \delta(q_1, 0) = q_0, \delta(q_1, 1) = q_1,$
 $\tilde{\pi}(q_0) = (.3, .7), \tilde{\pi}(q_1) = (.7, .3),$
2. $\delta(q_0, 0) = q_0, \delta(q_0, 1) = q_1, \delta(q_1, 0) = q_1, \delta(q_1, 1) = q_0,$
 $\tilde{\pi}(q_0) = (.3, .7), \tilde{\pi}(q_1) = (.7, .3),$
3. $\delta(q_0, 0) = q_1, \delta(q_0, 1) = q_2, \delta(q_1, 0) = q_2, \delta(q_1, 1) = q_0,$
 $\delta(q_2, 0) = q_0, \delta(q_2, 1) = q_1,$
 $\tilde{\pi}(q_0) = (.3, .7), \tilde{\pi}(q_1) = (.7, .3), \tilde{\pi}(q_2) = (.6, .4),$
4. $\delta(q_0, 0) = q_0, \delta(q_0, 1) = q_1, \delta(q_1, 0) = q_2, \delta(q_1, 1) = q_3,$
 $\delta(q_2, 0) = q_0, \delta(q_2, 1) = q_1, \delta(q_3, 0) = q_2, \delta(q_3, 1) = q_3,$
 $\tilde{\pi}(q_0) = (.3, .7), \tilde{\pi}(q_1) = (.7, .3),$
 $\tilde{\pi}(q_2) = (.8, .2), \tilde{\pi}(q_3) = (.2, .8).$

and the distance between coordinates to be the total variation distance (l_1 distance). One thing we'd like to point out is that, we used the aforementioned PFSA as base primarily for simplicity, and a more prudent way of forming the base, especially for supervised problems, would be to use the ensemble composed of one or more PFSA inferred from each class of the training dataset, using inference algorithm such as GenESeSs proposed in Sec. 4.

To evaluate the quality of a distance on a given training dataset of sequences, we first need to calculate the distance matrix D on the set, with $D_{i,j}$ being the distance between the i -th sequence and j -th sequence. Assuming that there are n sequences in the set and l_i is the label of the i -th sequence, we define the *average inter-class distances* to be

$$s(D) = \frac{\sum_{i=1}^n \sum_{j=1}^n \delta_{l_i l_j} D_{i,j}}{\sum_{i=1}^n \sum_{j=1}^n \delta_{l_i l_j}},$$

and *average intra-class distance* to be

$$d(D) = \frac{\sum_{i=1}^n \sum_{j=1}^n (1 - \delta_{l_i l_j}) D_{i,j}}{\sum_{i=1}^n \sum_{j=1}^n (1 - \delta_{l_i l_j})},$$

where $\delta_{ab} = 1$ if $a = b$ and 0 if otherwise. Now we can evaluate the quality of a distance matrix D by the ratio $r(D) = s(D)/d(D)$. The intuition behind this quality measurement is that a good distance metric should assign, on average, smaller distances to pairs of samples from the same class and larger distances to pairs of samples from different classes. The same quality measurement of quantization schemes was also discussed in the supplementary material to [4].

6.3 Smash, Smash2.0, and fastDTW

In this section we compare three time series distances, fastDTW proposed in [26], Smash proposed in [4], and Smash2.0 proposed in this paper. We show using a synthetic dataset that Smash2.0 outperforms the other two algorithms in both performance and efficiency. The dataset we use contains two classes, each with 20 sequences of length 500 generated by the two PFSA, G and H , as shown in Fig. 8. The two PFSA are functionally different as shown by their their KL divergence. We have $\mathcal{D}_{\text{KL}}(G \parallel H) \approx 0.19677$ and $\mathcal{D}_{\text{KL}}(H \parallel G) \approx 0.20756$. For fastDTW, we use the Python

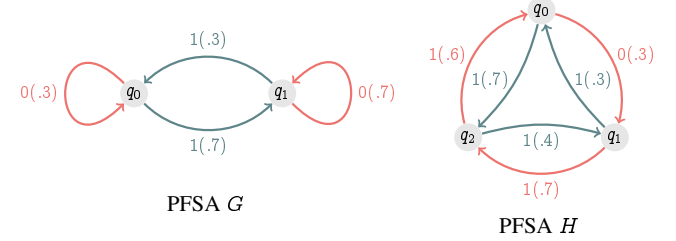


Fig. 8: PFSA that generate sequences for the comparison Sec. 6.3.

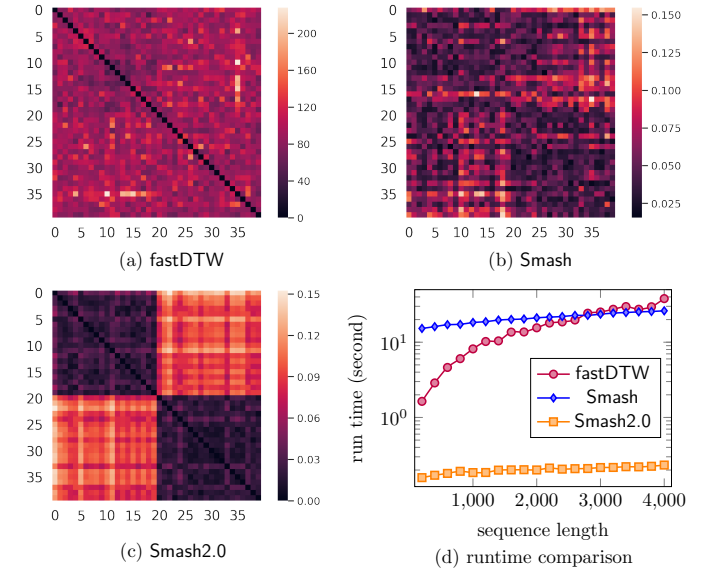


Fig. 9: Figure (a-c) are heatmaps of the distance matrices calculated by fastDTW, Smash, and Smash2.0. We can see that although the two PFSA generate drastically different stochastic processes, fastDTW fails to capture the distinction. Smash does a slightly better job than fastDTW, but Smash2.0 does much better. We show in (d) that Smash2.0 runs much faster than the other two algorithms.

package fastDTW (<https://pypi.org/project/fastdtw/>) with default value 1 for radius. We use 2 for number of reruns for Smash because of its probabilistic nature. In Fig. 9(a-c) we show the distance matrices given by the three algorithms using heatmaps. In Fig. 9 (d), we show running time of the three algorithms on dataset constructed the same way as above but with sequence length ranging from 200 to 4000, with 200 increment. The computer we used to do the calculation has Intel E5-2680v4 2.4GHz CPU and 64GB memory.

7 APPLICATIONS

In this section, we demonstrate the application of PFSA modeling and the log-likelihood technique to learning problems with sequential data.

7.1 Dataset 1: Motor Movement Imagery Dataset

This dataset is an excerpt of a dataset from PhysioNet[14]¹. The dataset contains 64-channel 160Hz EEG recorded by the BCI2000 system[27]² while subjects performed different motor/imagery

1. <http://www.physionet.org/pn4/eegmmidb/>
2. <http://www.bci2000.org>

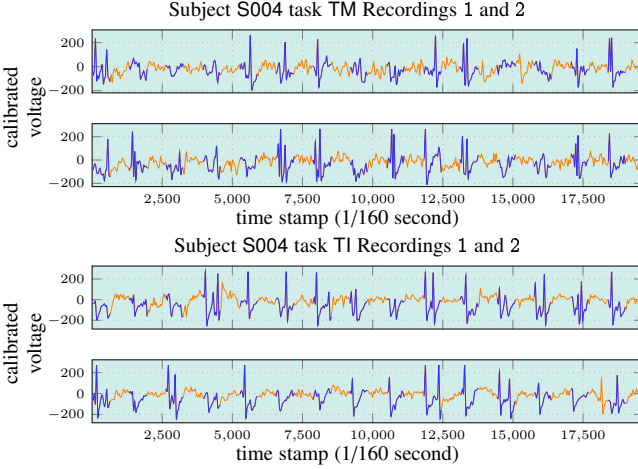


Fig. 10: EEG recordings of subject S004. The x -axis is sampling time stamp, and the y -axis is the magnitude of the reading.

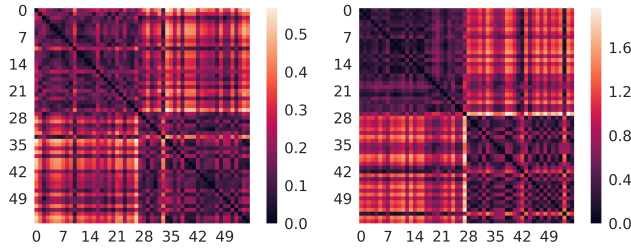


Fig. 11: Heatmaps for S004

tasks. There are four tasks included in the dataset and we focus on two of them:

TM: A target appears on either the left or the right side of the screen. The subject opens and closes the corresponding fist until the target disappears. Then the subject relaxes.

TI: The same as the first task, except the subject *imagines* opening and closing the corresponding fist but doesn't really move.

For each subject, three 2-minute EEG recordings are taken for each task and we use the first two recordings to get the results listed below. During each recording, an object appears on the screen for 4 seconds and disappear for 4 second, and hence a subject supposedly moves or imagines to move his or her fists for 4 seconds, then rest for 4 seconds, and repeat. In Fig. 10 and 12, the top two EEG recordings are for task TM and the bottom two, task TI. We color the rest sections blue, while the movement/imaginary movement sections orange.

For each subject we form a dataset with 56 sequence for each task, whose composition is detailed in Tab. 4. We drop the first section and the last section from each recordings since they tend to be more noisy.

seq.	TM dataset	TI dataset
0-13	rest from rec. 1	rest from rec. 1
14-27	rest from rec. 2	rest from rec. 2
28-41	movement from rec. 1	<i>imaginary</i> movement from rec. 1
42-55	movement from rec. 2	<i>imaginary</i> movement from rec. 2

TABLE 4: The composition of the TM and TI datasets

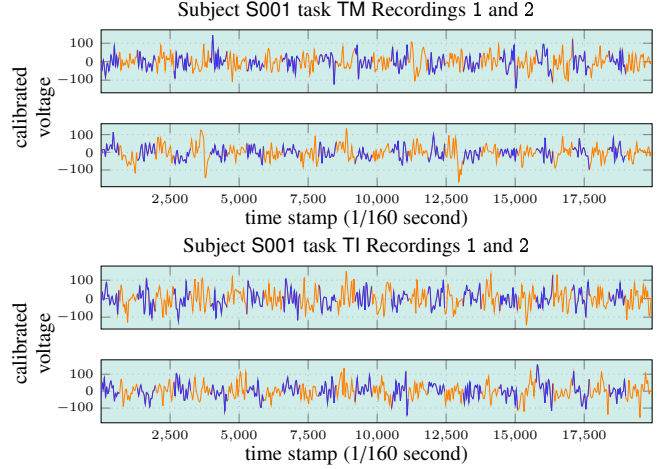


Fig. 12: EEG recordings of subject S001. The x -axis is sampling time stamp, and the y -axis is the magnitude of the reading.

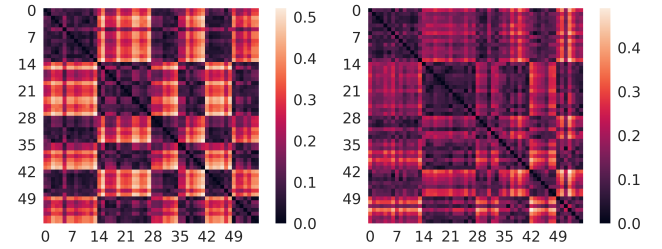


Fig. 13: Heatmaps for S001 for tasks TM and TI

The heatmap on the left of Fig. 11 demonstrates the distance matrix calculated from channel 25 of the subject S004 on task TM. The quantization scheme of the sequences is D0N1[-0.4526], with $r(D) = .572$. The heatmap on the right of Fig. 11 demonstrates the distance matrix calculated from channel 21 of the same subject on task TI. The quantization scheme is D0N0[-15.], with $r(D) = .451$. We can see that subject S004 has drastically different patterns in EEG between rest and (imaginary)movement sections, both from the wave and from the heatmaps of the distance matrices. The rest-movement difference of EEG is persistent across recordings as the distance between both the rest and movement sections from the first and second recordings are relatively insignificant.

The heatmap on the left of Fig. 13 demonstrates the distance matrix calculated from channel 41 of subject S001 on task TM. The quantization scheme of the sequences is D0N0[14.] with $r(D) = .825$. The heatmap on the right Fig. 13 demonstrates the distance matrix calculated from channel 59 of the same subject on task TI. The quantization scheme is D1N1[.4617], with $r(D) = .830$. We can see that subject S001 does not have significant difference in the EEG between rest and (imaginary) movement sections. Instead the subject seem to be in very different brain states during the two recordings for the same task.

7.2 Dataset 2: User Identification from Walking Activity

This dataset from UCI machine learning repository [11] contains 22 subject walking along a predefined trail in the wild. Accelerometer measurement in x, y, z directions was taken with an Android smartphone placed in the chest pocket of each participant. The challenge is to identify a user using his or her pattern of motion.

To form a training dataset for each subject, we get 10 sequence from the beginning of the measurement, each of 500 time steps long (each time step is about 0.03 second) and with 250 time step overlap between two consecutive sequences. There are 12 participants who has long enough measurement to form training datasets described above.

In Fig. 14, 15, and 16, we plot the heatmaps of the best two distances for acceleration measurement in the x , y , and z directions, respectively. Although the distance matrices calculated on all 12 participants, we demonstrate the heatmaps for the first 5 participants for clarity.

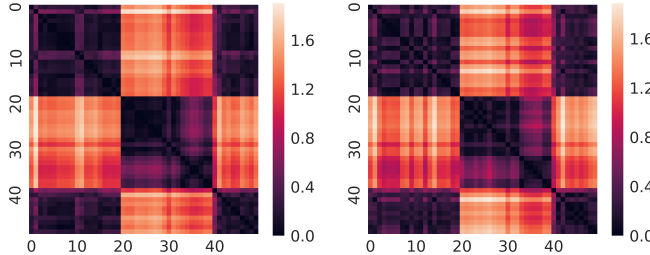


Fig. 14: Heatmaps for best two distances in x direction. On left: D0N0[-1.1169] with $r(D) = .230$. On right: D0N0[-0.3814] with $r(D) = .248$.

From this example we can see that although it may be difficult to tell two participant apart by using measurement from one directions, using measurement from multiple channels combined with the freedom of our approach to choose quantization schemes customized for each individual channel, we may boost the classification performance. As for an example, while the distance in the x direction between the first two participants (sequences 0-9, and sequences 10-19) may not be great enough to tell them apart, their patterns of motion in the z direction do have much big distinction as indicated by the the first 20 by 20 diagonal block of the two heatmaps in Fig. 16.

8 CONCLUSION

In this paper, we propose a distance metric Smash2.0 between time series based on PFSA modeling and sequence likelihood divergence. We give a self-contained introduction to the mathematical foundation of PFSA as a time series model, the quantification of entropy rate and KL divergence of the stochastic process generated by PFSA, and finally, log-likelihood convergence of sample paths. We show how to infer PFSA from sequences and how to evaluate sequence likelihood divergence using log-likelihood convergence. We define the distance metric Smash2.0 using sequence likelihood divergence, and with the help of quantization algorithm of continuous data streams, we demonstrate how to apply Smash2.0 to the analysis of time series datasets arising from real world scenarios.

Possible future research effort includes 1) finding a better way to choose base PFSA for the Smash2.0 in unsupervised settings; 2) finding a base-free way to calculate Smash2.0 distance by, for example, inferring a PFSA model from each time series in the dataset.

REFERENCES

- [1] J. BONDY AND U. MURTY, *Graph theory* (2008), Grad. Texts in Math. (2008).
- [2] I. CHATTOPADHYAY, *Causality networks*, arXiv preprint arXiv:1406.6651, (2014).
- [3] I. CHATTOPADHYAY AND H. LIPSON, *Abductive learning of quantized stochastic processes with probabilistic finite automata*, Philosophical Transactions of the Royal Society A: Mathematical, Physical and Engineering Sciences, 371 (2013), p. 20110543.
- [4] ———, *Data smashing: uncovering lurking order in data*, Journal of The Royal Society Interface, 11 (2014), p. 20140826.
- [5] I. CHATTOPADHYAY AND A. RAY, *Structural transformations of probabilistic finite state machines*, International Journal of Control, 81 (2008), pp. 820–835.
- [6] L. CHEN, M. T. ÖZSU, AND V. ORIA, *Robust and fast similarity search for moving object trajectories*, in Proceedings of the 2005 ACM SIGMOD international conference on Management of data, ACM, 2005, pp. 491–502.
- [7] W. CHING AND M. Ng, *Markov Chains: Models, Algorithms and Applications*, International Series in Operations Research & Management Science, Springer US, 2006.
- [8] T. M. COVER AND J. A. THOMAS, *Elements of information theory*, John Wiley & Sons, 2012.
- [9] J. P. CRUTCHFIELD, *The calculi of emergence: computation, dynamics and induction*, Physica D: Nonlinear Phenomena, 75 (1994), pp. 11–54.
- [10] J. DOOB, *Stochastic processes*, Wiley publications in statistics, Wiley, 1990.
- [11] D. DUA AND C. GRAFF, *UCI machine learning repository*, 2017.
- [12] P. DUPONT, F. DENIS, AND Y. ESPOSITO, *Links between probabilistic automata and hidden markov models: probability distributions, learning models and induction algorithms*, Pattern recognition, 38 (2005), pp. 1349–1371.
- [13] P. A. GAGNIUC, *Markov chains: from theory to implementation and experimentation*, John Wiley & Sons, 2017.
- [14] A. L. GOLDBERGER, L. A. AMARAL, L. GLASS, J. M. HAUSDORFF, P. C. IVANOV, R. G. MARK, J. E. MIETUS, G. B. MOODY, C.-K. PENG, AND H. E. STANLEY, *Physiobank, physiotoolkit, and physionet: components of a new research resource for complex physiologic signals*, Circulation, 101 (2000), pp. e215–e220.
- [15] L. C. KAI, *Markov Chains: With Stationary Transition Probabilities*, Springer-Verlag, 1967.
- [16] D. P. KINGMA AND M. WELLING, *Auto-encoding variational bayes*, arXiv preprint arXiv:1312.6114, (2013).
- [17] A. KLENKE, *Probability theory: a comprehensive course*, Springer Science & Business Media, 2013.
- [18] J. LIN, E. KEOGH, S. LONARDI, AND B. CHIU, *A symbolic representation of time series, with implications for streaming algorithms*, in Proceedings of the 8th ACM SIGMOD workshop on Research issues in data mining and knowledge discovery, ACM, 2003, pp. 2–11.

[19] A. G. D. G. MATTHEWS, J. HENSMAN, R. TURNER, AND Z. GHAHRAMANI, *On sparse variational methods and the kullback-leibler divergence between stochastic processes*, Journal of Machine Learning Research, 51 (2016), pp. 231–239.

[20] C. S. MÖLLER-LEVET, F. KLAWONN, K.-H. CHO, AND O. WOLKENHAUER, *Fuzzy clustering of short time-series and unevenly distributed sampling points*, in International Symposium on Intelligent Data Analysis, Springer, 2003, pp. 330–340.

[21] G. NAVARRO, *A guided tour to approximate string matching*, ACM computing surveys (CSUR), 33 (2001), pp. 31–88.

[22] P. Z. PEEBLES, *Probability, random variables, and random signal principles*, vol. 3, McGraw-Hill New York, NY, USA:, 2001.

[23] F. PETITJEAN, A. KETTERLIN, AND P. GANÇARSKI, *A global averaging method for dynamic time warping, with applications to clustering*, Pattern Recognition, 44 (2011), pp. 678–693.

[24] S. S. RAY, *Graph theory with algorithms and its applications: in applied science and technology*, Springer Science & Business Media, 2012.

[25] D. J. REZENDE, S. MOHAMED, AND D. WIERSTRA, *Stochastic backpropagation and approximate inference in deep generative models*, arXiv preprint arXiv:1401.4082, (2014).

[26] S. SALVADOR AND P. CHAN, *Fastdtw: Toward accurate dynamic time warping in linear time and space*, in KDD workshop on mining temporal and sequential data, Citeseer, 2004.

[27] G. SCHALK, D. J. MCFARLAND, T. HINTERBERGER, N. BIRBAUMER, AND J. R. WOLPAW, *Bci2000: a general-purpose brain-computer interface (bci) system*, IEEE Transactions on biomedical engineering, 51 (2004), pp. 1034–1043.

[28] M. STAMP, *A revealing introduction to hidden markov models*, Department of Computer Science San Jose State University, (2004), pp. 26–56.

[29] S. Y. YAN, *An introduction to formal languages and machine computation*, World Scientific, 1998.